International Journal of Multiphase Flow 35 (2009) 205–218

Contents lists available at ScienceDirect

International Journal of Multiphase Flow

journal homepage: www.elsevier.com/locate/ijmulflow

Infiltration of liquid droplets into porous media: Effects of dynamic contact angle and contact angle hysteresis

Markus Hilpert [a,*], Avishai Ben-David [b]

[a] Johns Hopkins University, Department of Geography and Environmental Engineering, Baltimore, MD 21218, USA
[b] Edgewood Chemical Biological Center, Research Development and Engineering Command, Aberdeen Proving Ground, MD 21010, USA

ARTICLE INFO

Article history:
Received 11 August 2008
Received in revised form 24 October 2008
Accepted 27 November 2008
Available online 24 December 2008

ABSTRACT

We present a detailed theory for infiltration, which accounts for a general model for the dynamic contact angle between the droplet and the porous medium as well as contact angle hysteresis, and analyze the resulting equations of motion. The theory shows that infiltration of droplets into dry porous media involves three phases due to contact angle hysteresis: (1) An increasing drawing area (IDA) phase during which the interface between the droplet and the porous medium increases, (2) a constant drawing area (CDA) phase during which the contact line of the droplet remains pinned, and (3) a decreasing drawing area (DDA) phase. The theory is based on the following assumptions: (1) The droplet has the shape of a spherical cap, (2) the porous medium consists of a bundle of vertical tubes of same size, and (3) the pressure within the droplet is uniform. We find that infiltration always consists of a cascade process formed by the IDA, CDA, and DDA phases, where the entire process may begin or end in any of the three phases. The entire process is formulated with four nondimensional parameters: Three contact angles (initial, advancing, and receding) and a porous permeability parameter. A comparison of our theory to experimental data suggests that one should use different parameterizations for the dynamic contact angle models of the IDA and DDA phases. In general, the IDA and DDA phases are described by integro-differential equations. A numerical-solution approach is presented for solving the dynamic equations for infiltration. The total time of infiltration and the time dependence of drawing area are critically affected by the occurrence of the IDA, CDA, and DDA phases as well as by the permeability. With ordinary differential equations (ODEs), we are able to approximate the IDA phase and to describe exactly infiltration processes that start out with the CDA or DDA phase.

1. Introduction

Infiltration of liquid droplets into dry porous media occurs in industrial and natural settings: When rain drops fall onto soil, in ink jet printers, when accidentally spilling organic liquid (e.g., gasoline and chlorinated solvents) onto ground, and when aerosol pesticides are not intercepted by the vegetation and then released to soils. In these scenarios, it is important to know how droplet infiltration occurs. For instance, if harmful chemicals are released from the droplet into the atmosphere through evaporation, it is important to know the time of infiltration. In printing applications, a goal is to quantify the dynamics of the area wetted by the droplet.

Hence, models that predict how a droplet infiltrates into a porous medium have been developed. Denesuk et al. (1993) developed a model that (1) represents the porous medium by a bundle of vertically oriented capillary tubes, (2) treats the model porous medium in a continuum fashion, and (3) assumes the droplet to have the shape of a spherical cap. See Fig. 1 for the geometry. For systems that are not totally wetting (no "remnant" films), Denesuk et al. (1993) investigated two "limiting" scenarios:

1. A decreasing drawing area (DDA) case, during which the area between the droplet and the porous medium which withdraws liquid from the droplet, decreases while the contact angle of the droplet, θ, remains constant.
2. A constant drawing area (CDA) case, during which θ decreases until the droplet is depleted (when $\theta \to 0^\circ$). The contact line is pinned (does not move) during the CDA phase.

Later, Holman et al. (2002) built on the work by Denesuk et al. (1993) and allowed for an increasing drawing area. We refer to this process as the IDA phase. In order to describe this spreading process, Holman et al. (2002) employed the following equation for the drawing radius R_d of the drop: $R_d(t) = (a + bt)^n$ where t is time, and a, b, and n are constants. This relation indirectly causes the contact angle θ to depend on time t. The theory developed by Holman et al. (2002) has an integrable solution and is appropriate, when predictions of droplet infiltration are being inferred from the drawing radius observed as a function of time, $R_d(t)$. Predictions

* Corresponding author.
E-mail address: markus_hilpert@jhu.edu (M. Hilpert).

0301-9322/$ - see front matter © 2008 Elsevier Ltd. All rights reserved.
doi:10.1016/j.ijmultiphaseflow.2008.11.007

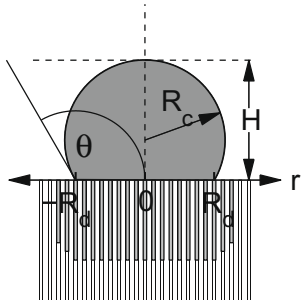

Fig. 1. Geometry of a droplet sitting on a porous surface, where R_d is the drawing radius. In this example, the drawing area decreases. Hence, the vertical capillary tubes for $r > R_d$ have withdrawn less liquid.

based on initial conditions are, however, not possible. In the model presented here, we will remedy this limitation.

The Denesuk et al. (1993) and Holman et al. (2002) models describe infiltration events that consist of either the IDA, CDA, or DDA phase but not of a combination of these phases because of assumptions made about the values of the equilibrium advancing contact angle θ_a and the equilibrium receding contact angle θ_r. Denesuk et al.'s (1993) model for the CDA phase implicitly assumes $\theta_r = 0°$, while Holman et al.'s (2002) model implicitly assumes $\theta_a = 0°$. On porous surfaces, however, θ_a and θ_r may assume non-zero values (Bachmann et al., 2003).

Experiments (Bacri and Brochard-Wyart, 2000; Clarke et al., 2002; Zhdanov et al., 2003) have shown that the IDA, CDA, and DDA phases may all occur during a single infiltration event. In a recent Letter, Clarke et al. (2002) presented a theory that accounts for a law for dynamic contact angle based on molecular-kinetic theory and a general model for contact angle hysteresis. Consistent with infiltration experiments, Clarke et al. (2002) postulated that droplet infiltration involves the IDA, CDA, and DDA phases and that the phases presumably occur subsequently.

The scope of this paper is to present a detailed theory for infiltration of a droplet into a porous medium. The theory will account for contact angle hysteresis and clearly show how θ_a and θ_r enter the equations of motion. Note that we do not address infiltration in totally wetting systems (Alleborn and Raszillier, 2004; Daniel et al., 2006; Zadrazil et al., 2006), for which the spreading coefficient is $\geqslant 0$ and hysteresis does not occur. We will show that infiltration occurs in the following three phases (see Fig. 2) and prove that these phases occur exactly in that order, where the entire process may begin or end in any of the three phases:

1. In the IDA phase, the initial contact angle of the drop, $\theta_i = \theta(t = 0)$, is assumed to be larger than θ_a and R_d increases. As the velocity of the contact line, $\dot{R}_d$, gradually becomes smaller, θ decreases until it assumes θ_a at time $t = t_a$.
2. In the CDA phase, the contact line remains pinned while θ decreases until it assumes θ_r at time $t = t_r$.
3. In the DDA phase, the contact line starts moving again. R_d decreases until the droplet is depleted at the final time $t = t_f$.

Furthermore, we will

1. account for a general class of models for dynamic contact angle;
2. present a comprehensive dimensional analysis;
3. discuss the limits of validity of our theory with respect to the spherical cap assumption and neglecting gravity;
4. present approaches for representing the equations of motion by integro-differential equations and ordinary differential equations (ODEs);
5. present a numerical-solution approach for our theory; and
6. compare our theory to experiments, from which we draw conclusions on the behavior of dynamic contact angle on porous surfaces.

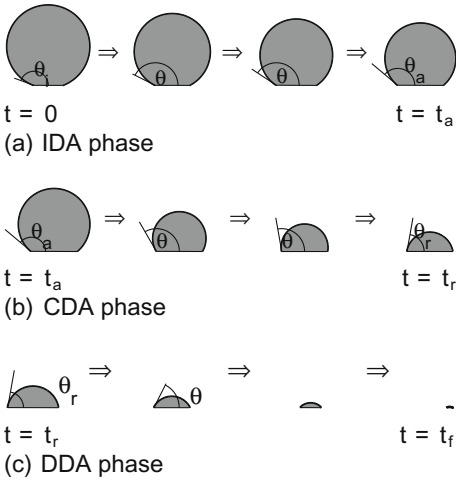

Fig. 2. Infiltration occurs in three phases. (a) During the IDA phase, the drawing radius R_d increases while the contact angle of the droplet θ decreases until it assumes the advancing contact angle θ_a. (b) During the CDA phase, θ decreases from θ_a until it assumes the receding contact angle θ_r while R_d = const. (c) During the DDA phase, R_d decreases until the droplet is depleted.

2. Model for infiltration

2.1. Modeling assumptions

2.1.1. Porous medium

We build on the work of Denesuk et al. (1993) and model the porous medium by a bundle of vertically oriented capillary tubes. The tubes withdraw liquid from the droplet as shown in Fig. 1.

2.1.2. Mass conservation

Neglecting evaporation and assuming incompressibility of the liquid, the total volume of liquid, V_0, remains constant during infiltration,

$$V_0 = V_d(t) + V_p(t) \tag{1}$$

where V_p is the volume of liquid in the porous medium, and V_d is the volume of the droplet.

2.1.3. Spherical cap assumption

We assume radial symmetry. Moreover, the droplet is assumed to have the shape of a spherical cap. Hence, the volume of the droplet is (Denesuk et al., 1993)

$$V_d = \xi(\theta) R_d^3 \tag{2}$$

where

$$\xi(\theta) = \frac{\pi}{3} \frac{(1 - \cos\theta)(\cos\theta + 2)}{\sin\theta(\cos\theta + 1)} \tag{3}$$

The radius of curvature of the droplet is

$$R_c = \frac{R_d}{\sin\theta} \tag{4}$$

The height of the droplet is

$$H = R_c(1 - \cos\theta) \tag{5}$$

Fig. 3 shows ξ and

$$\frac{d\xi}{d\theta} = \frac{\pi}{(1 + \cos\theta)^2} \tag{6}$$

One can show that $d\xi/d\theta > 0$ for $0 \leqslant \theta < 180°$.

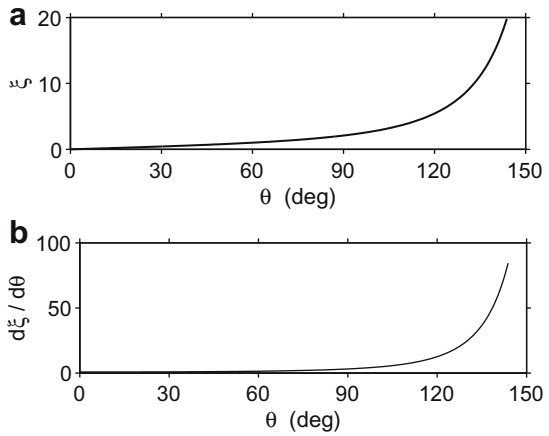

Fig. 3. Dependence of the ξ function, which is used to calculate the droplet volume according to Eq. (2), and its derivative on contact angle θ.

The spherical cap approximation assumes internal flow to have negligible impact on droplet shape. Should a spherical droplet be administered to the porous surface with an impingement velocity v_i, then the assumption is justified if the Weber number (ratio of typical inertial to capillary forces) $We = \rho R_0 v_i^2/\gamma$ is small where ρ is the liquid density, R_0 is the radius of the droplet, and γ is surface tension.

The spherical cap assumption moreover requires gravity to be negligible. According to the hydrostatic pressure distribution, gravity causes a difference in liquid pressure between the surface of the porous medium and the top of the liquid droplet, $\Delta p_l = \rho g H$, where g is gravitational acceleration. This pressure difference causes capillary pressure p_c to vary on the droplet surface. Because the air pressure is about constant (due to the low density of air), the capillary pressure difference between the top and bottom of the droplet is $\Delta p_l = |\Delta p_c|$. The variation in p_c causes the radii of curvature of the air–liquid interface to be nonuniform, i.e., non-sphericity. The effects of gravity on droplet sphericity are negligible if $|\Delta p_c| \ll p_c$ where $p_c = 2\gamma/R_c$ is the capillary pressure of the droplet with the shape of a spherical cap. Using Eq. (5), the condition for a spherical cap becomes

$$\frac{|\Delta p_c|}{p_c} = \frac{\rho g H^2}{2\gamma}\frac{1}{1-\cos\theta} \ll 1 \tag{7}$$

Note that this condition is fulfilled even if $\theta \to 0$, because then $H \to 0$ and hence $|\Delta p_c|/p_c \to 0$.

The validity of Inequality (7) during an entire infiltration event can be verified by evaluation of the initial conditions, because the droplet height H, more or less, decreases with time t. For example, for silicone oil from Table 1, a droplet height $H = 1$ mm, and a contact angle $\theta = 90°$, $|\Delta p_c|/p_c \approx 0.22$, i.e., gravity has negligible impact on droplet shape. In the simulation presented in this paper, Inequality (7) is always fulfilled.

2.1.4. Neglecting gravity when modeling flow in tubes

We model flow in the tubes with Washburn's (1921) equation. For mathematical convenience, we, like Denesuk et al. (1993) and Holman et al. (2002), do not account for the effects of gravity on flow by assuming the tubes to be horizontally oriented when modeling flow. The liquid pressure at the tube inlet is assumed to equal atmospheric pressure. When infiltration starts at time $t = 0$, the length of the liquid slug in the tube as a function of time t is

$$h(t) = A\sqrt{t} \tag{8}$$

where

$$A = \sqrt{\frac{R_t \gamma \cos\alpha}{2\eta}} \tag{9}$$

R_t is the tube radius, η is the dynamic viscosity, and α is the equilibrium contact angle in the tubes that represent the porous medium. We assume $\alpha < 90°$; otherwise liquid is not sucked into the tubes.

Washburn (1921) derived a general solution that also accounts for gravity. For vertical downward infiltration, Washburn (1921) obtained

$$\frac{h}{h_0} - \frac{t}{t_0} = \ln\left(1 + \frac{h}{h_0}\right) \tag{10}$$

where we nondimensionalized the solution by introducing a length scale $h_0 = 2\gamma\cos\alpha/(\rho g R_t)$ and a time scale

$$t_0 = 16\frac{\gamma\eta\cos\alpha}{\rho^2 g^2 R_t^3} \tag{11}$$

Neglecting gravity is permissible for infiltration times

$$t \ll t_0 \tag{12}$$

because then the $\ln(\ldots)$ term can be expanded in a Taylor series that retains terms only up to second order. This results in the solution given by Eq. (8).

Strictly speaking, one first needs to solve our model for infiltration numerically in order to check whether Inequality (12) is fulfilled. If the infiltration duration is not much smaller than t_0, the solution for times not much smaller than t_0 is deficient. For the silicone oil from Table 1, a tube size of $R_t = 0.1$ mm, a tube contact angle $\alpha = 0°$, we obtain $t_0 = 1$ h. This time scale exceeds by far the durations of the infiltration simulations presented in this paper. Hence, we can safely assume that Inequality (12) is fulfilled.

2.1.5. Continuum representation of the porous medium

Assuming that $R_d \gg R_t$ we can treat the porous medium as a continuum of porosity ϵ. To calculate V_p we first quantify the liquid volume that, at time t, has infiltrated into the porous medium through a ring with radius r and infinitesimally small width dr:

$$dV_p(t) = \epsilon 2\pi r h(t_i(r,t))dr \tag{13}$$

where $t_i(r,t)$ is the period of time for which infiltration has occurred at radial position r and at time t. The total volume of liquid in the porous medium at time t is:

$$V_p(t) = \int_0^\infty \frac{dV_p}{dr}dr = 2\pi\epsilon\int_0^\infty r h(t_i(r,t))dr \tag{14}$$

Even if the continuum condition $R_d \gg R_t$ is initially fulfilled, it may be violated in a later stage of infiltration. One must be cautious about using a continuum model for small droplet sizes, but if one does, it makes sense to assume infiltration to be terminated when

$$R_d = R_t \tag{15}$$

because then the droplet "falls" into a tube of the porous medium.

2.1.6. Constant pressure in the droplet

Denesuk et al. (1993) as well as we assumed that the liquid pressure in the droplet remains constant during infiltration and is equal to atmospheric pressure p_a. In reality, the differential equation for infiltration into a horizontal tube is (Washburn, 1921):

Table 1
Liquid properties of SF-96 silicone oil at a temperature of 25 °C (Hoffman, 1975).

Dynamic viscosity η	0.958 kg/(m s)
Surface tension γ	21.3×10^{-3} N/m
Density ρ	971 kg/m^3

$$\frac{dh}{dt} = \left(p_{l,0} - p_a + \frac{2\gamma}{R_t}\cos\alpha\right)\frac{R_t^2}{8\eta h} \tag{16}$$

where $p_{l,0}$ is the liquid pressure at the tube inlet (the upper surface of the porous medium). Here we slightly generalized the equation derived by Washburn (1921, Eq. (9)) who assumed that a liquid reservoir, of depth d and with a flat air–liquid interface, supplies liquid to a horizontal capillary tube. Using our notation, he wrote $\rho g d$ instead of $p_{l,0} - p_a$. The solution given by Eq. (8) assumes that d does not depend on time t and specifically that $d = 0$, that is, $p_{l,0} = p_a$. We can neglect the $p_{l,0} - p_a$ term in Eq. (16) only if $|p_{l,0} - p_a| \ll 2\gamma\cos\alpha/R_t$. Using the fact that $p_{l,0} - p_a$ is the capillary pressure $2\gamma/R_c$ and using Eq. (4), we can rewrite the condition that allows us to assume constant pressure in the droplet as follows:

$$R_d\cos\alpha \gg R_t\sin\theta \tag{17}$$

Note that both R_d and θ depend on time t.

If $R_d \to R_t$, as is possible during the final stages of the DDA phase, our theory may not be applicable as Inequality (17) is not fulfilled. If our theory is implemented when Inequality (17) is violated, the solution will underestimate the rate of infiltration. If α is small, then the condition is more likely to be fulfilled, potentially for the entire infiltration event. Also if $\theta(t)$ is small toward the end of infiltration, the condition is more likely to be fulfilled. When presenting simulation results, we will indicate when Inequality (17) is not fulfilled.

2.1.7. Dynamic contact angle

We assume that the dynamic contact angle θ is described by the following general model F:

$$\theta = F(\hat{v}, \theta_0) \tag{18}$$

where

$$\hat{v} = \frac{\eta v}{\gamma} \tag{19}$$

is the nondimensional (positive) contact line velocity, v is the dimensional (positive) contact line velocity, and θ_0 is the equilibrium contact angle.

Little is known about which functional form to use for F on porous surfaces. For impermeable surfaces, Cox (1986) derived a functional form for F that is consistent with Eq. (18). For that, Cox (1986) used basic fluid-mechanical principals, including a no-slip condition (zero-fluid velocity) on the solid surface, except in the vicinity of the three-phase contact line where fluid slip is assumed to occur.

Since the no-slip condition assumed by Cox (1986) is not fulfilled on a porous surface and since Cox' (1986) model for F is defined through an integral, this paper uses two empirical relations for F that possess simpler functional forms. The first relation was proposed by Jiang et al. (1979), who analyzed capillary tube experiments, which Hoffman (1975) performed with five different liquids:

$$\cos\theta = \cos\theta_0 - (1 + \cos\theta_0)\tanh(4.96\cdot\hat{v}^{0.702}) \tag{20}$$

The second relation is the Hoffman–Voinov–Tanner law

$$\theta^3 - \theta_0^3 = c_t\hat{v} \tag{21}$$

where $c_t \approx 72$ (Šikalo et al., 2005). An advantage of Eq. (20) over Eq. (21) is that Eq. (20) conforms to the upper geometrical bound for the contact angle, $\theta \leqslant 180°$. Note that in Eqs. (20) and (21) both θ and θ_0 are measured in the advancing fluid. Also in both cases, F increases monotonically with $\hat{v}$,

$$\frac{dF}{d\hat{v}} > 0 \tag{22}$$

Hence, F can be inverted. For the model given by Eq. (20) one obtains

$$\hat{v}(\theta,\theta_0) = F^{-1}(\theta,\theta_0) = \left[\frac{1}{4.96}\tanh^{-1}\left(\frac{\cos\theta_0 - \cos\theta}{1+\cos\theta_0}\right)\right]^{1/0.702} \tag{23}$$

and

$$\frac{dF}{d\hat{v}} = 4.96\cdot 0.702\cdot\hat{v}^{-0.298}\frac{1+\cos\theta_0}{\sin\theta}\operatorname{sech}^2(4.96\cdot\hat{v}^{0.702}) \tag{24}$$

For the model given by Eq. (21) one obtains

$$\hat{v}(\theta,\theta_0) = F^{-1}(\theta,\theta_0) = \frac{\theta^3 - \theta_0^3}{c_t} \tag{25}$$

and

$$\frac{dF}{d\hat{v}} = \frac{c_t}{3\theta^2} \tag{26}$$

We note that Davis and Hocking (2000), who performed a theoretical study that assumes a constant microscopic equilibrium contact angle of 1° and uses the lubrication approximation for flow in the droplet, even question Eq. (18), that is, that θ is a single-valued function of $\hat{v}$. Their theory, however, still lacks experimental support. Moreover, it is not clear whether their findings also apply to equilibrium contact angles other than 1° and how to account for contact angle hysteresis. Hence, our analysis builds on Eq. (18).

2.1.8. Contact angle hysteresis

Contact angle hysteresis occurs due to chemical heterogeneity and surface roughness and causes a non-unique equilibrium contact angle θ_0, which is bound between the advancing contact angle θ_a and the receding contact angle θ_r. The actual contact angle θ can change between θ_a and θ_r without any contact line movement, as is the case during the CDA phase and as is illustrated in Fig. 4b. If $\theta > \theta_a$, then the contact line moves outwards as shown in Fig. 4a, the IDA phase is assumed, and the dynamic contact angle θ is, according to Eq. (18), given by

$$\theta = F_a\left(\frac{\eta\dot{R}_d}{\gamma}, \theta_a\right) \tag{27}$$

where the subscript a in F_a indicates that this model is parameterized by θ_a. If $\theta < \theta_r$, then the contact line moves inwards as shown in Fig. 4c, the DDA phase is assumed, and the dynamic contact angle θ is given by

$$\pi - \theta = F_r\left(-\frac{\eta\dot{R}_d}{\gamma}, \pi - \theta_r\right) \tag{28}$$

where the subscript r in F_r indicates that this model is parameterized by θ_r. Note that the droplet contact angles θ and θ_0 enter Eq. (18) as $\pi - \theta$ and $\pi - \theta_r$, respectively, because the two contact angles in Eq. (18) are measured in the advancing fluid, which is the gas phase during the DDA phase. Further, $\dot{R}_d < 0$ enters Eq. (18)

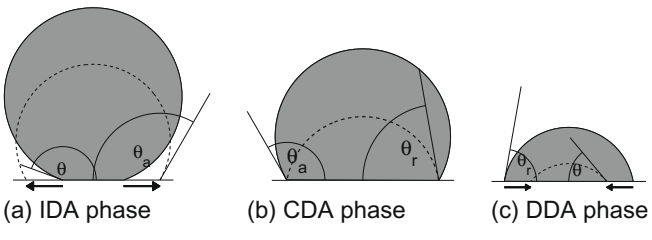

Fig. 4. (a) During the IDA phase, the drawing radius R_d increases, and $\theta \geqslant \theta_a$. (b) During the CDA phase, R_d is constant, and θ varies between θ_a and θ_r. (c) During the DDA phase, R_d decreases, and $\theta \leqslant \theta_r$.

with a minus sign, because the velocity in Eq. (18) is positive. We expect different parameterizations for F_a and F_r, because Cox (1986) has shown that the dynamic contact angle on impermeable surfaces depends on the ratio of viscosity between the advancing and receding fluid. It seems reasonable to assume that this also holds true for the permeable surfaces considered in this study.

The theory that we develop will only use Eqs. (27) and (28) but not specific parameterizations for F_a and F_r. Thus, our model assumes only that F_a and F_r are continuous and increase monotonically with the contact line velocity $\hat{v}$.

2.2. Infiltration during the IDA phase

We denote the time when infiltration begins at radial position r by $t_b(r)$. During the IDA phase, all tubes with radial position r within the initial drawing area withdraw liquid from the droplet starting at time $t = 0$, that is, $t_b(r) = 0$ for $0 \leqslant r \leqslant R_d(0)$. Tubes outside this region get invaded later on, that is, $t_b(r) > 0$ for $r > R_d(0)$. At time t, all tubes with r value smaller than the current (and increasing) drawing radius $R_d(t)$ will have withdrawn liquid from the droplet until that time t. Hence, at time t, infiltration will have occurred for a duration

$$t_i(r,t) = \begin{cases} t - t_b(r) & \text{for} \quad r \leqslant R_d(t) \\ 0 & \text{for} \quad r > R_d(t) \end{cases} \tag{29}$$

The duration t_i is larger for $r \leqslant R_d(0)$ than for $R_d(0) < r \leqslant R_d(t)$, because tubes in the latter region are not supplied with liquid at time $t = 0$ but need to wait until the expanding droplet starts feeding them with liquid. Fig. 5a illustrates t_b and t_i. Using Eqs. (14) and (29), the total volume of liquid in the porous medium becomes:

$$V_p(t) = 2\pi\epsilon \int_0^{R_d(t)} rh(t - t_b(r))dr \tag{30}$$

For the mathematical analysis, it is advantageous to recast Eq. (30) as follows:

$$\begin{aligned} V_p(t) &= 2\pi\epsilon \int_0^{R_d(t)} r \int_{t_b(r)}^{t} \dot{h}(\tau - t_b(r))d\tau dr \\ &= \pi A\epsilon \int_0^{R_d(t)} r \int_{t_b(r)}^{t} \frac{r}{\sqrt{\tau - t_b(r)}} d\tau dr \end{aligned} \tag{31}$$

The shaded area in Fig. 5a depicts the integration domain of the τ integral. We evaluate the double integral in Eq. (31) by changing the order of integration, similar to the analysis of Denesuk et al. (1993) for the DDA phase. For the IDA phase, however, we first need to eliminate the integration limit t_b in the integrand so that we can change the order of integration. This is done via the substitution $\tau' = \tau - t_b$:

$$V_p(t) = \pi A\epsilon \int_0^{R_d(t)} \int_0^{t - t_b(r)} \frac{r}{\sqrt{\tau'}} d\tau' dr \tag{32}$$

We now change the order of integration:

$$V_p(t) = \pi A\epsilon \int_0^{t} \int_0^{R_d(t-\tau)} \frac{r}{\sqrt{\tau}} dr d\tau = \frac{\pi A\epsilon}{2} \int_0^{t} \frac{R_d^2(t-\tau)}{\sqrt{\tau}} d\tau \tag{33}$$

Substituting the expressions for V_d and V_p given by Eqs. (2) and (33), respectively, into Eq. (1) yields:

$$\xi(\theta) R_d^3 + \frac{\pi A\epsilon}{2} \int_0^{t} \frac{R_d^2(t-\tau)}{\sqrt{\tau}} d\tau = V_0 \tag{34}$$

Together with Eq. (27) for θ during the IDA phase, we obtain an integro-differential equation for $R_d(t)$:

$$F_a\left(\frac{\eta \dot{R}_d}{\gamma}, \theta_a\right) = \xi^{-1}\left(\frac{1}{R_d^3}\left[V_0 - \frac{\pi A\epsilon}{2} \int_0^{t} \frac{R_d^2(t-\tau)}{\sqrt{\tau}} d\tau\right]\right) \tag{35}$$

It is intuitive that the contact line of the droplet slows down with time, because liquid, according to Eq. (8), is sucked into the porous medium in a diffusive manner. Indeed, one can show that the contact line decelerates. Substituting Eq. (2) into Eq. (1) and differentiating it with respect to t yields

$$\frac{d\xi}{d\theta} \frac{dF_a}{d\hat{v}} \frac{\eta}{\gamma} \ddot{R}_d = -\left(\frac{3\xi \dot{R}_d}{R_d} + \frac{\dot{V}_p}{R_d^3}\right) \tag{36}$$

Since $d\xi/d\theta > 0$, $\xi \geqslant 0$, $R_d > 0$, $dF_a/d\hat{v} > 0$, and $\dot{V}_p > 0$, it indeed follows that $\ddot{R}_d < 0$. Hence, the advancing contact line slows down. The IDA phase ends once $\theta(t) = \theta_a$ (when $\dot{R}_d = 0$) and is followed by the CDA phase described next (unless $\theta_a = 0$).

2.3. Infiltration during the CDA phase

For both the IDA and DDA phases, the liquid volume in the pore space is given by Eq. (33), because for both phases t_i is given by Eq. (29). Hence, by substituting Eq. (2) for the droplet volume and Eq. (33) into Eq. (1), one obtains an explicit expression for the contact angle:

$$\theta(t) = \xi^{-1}\left(\frac{1}{R_d^3(t_a)}\left[V_0 - \frac{\pi A\epsilon}{2} \int_0^{t} \frac{R_d^2(t-\tau)}{\sqrt{\tau}} d\tau\right]\right) \tag{37}$$

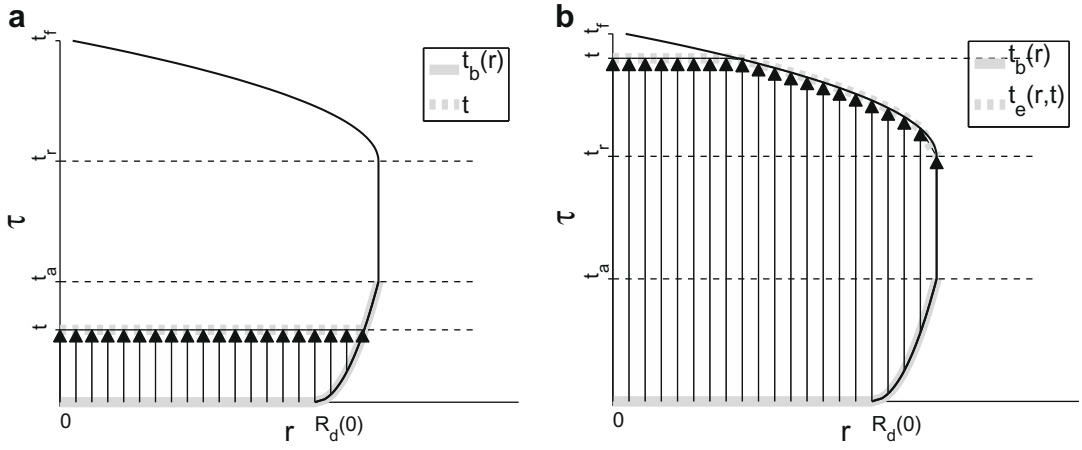

Fig. 5. (a) Illustration of the time t_b, at which infiltration begins in a tube a position r during the IDA phase. The arrows indicate the duration of infiltration, $t_i(r,t) = t - t_b(r)$, for tubes at position r and time t. (b) Illustration of the time t_e, at which infiltration ends in a tube a position r during the DDA phase. The arrows indicate $t_i(r,t) = t_e(r) - t_b(r)$. In both plots, the black solid line represents the drawing radius R_d as a function of the ordinate time τ.

Here, the R_d in the integrand is known:

$$R_d(t) = \begin{cases} R_{\mathrm{IDA}}(t) & \text{for} \quad t < t_a \\ R_d(t_a) & \text{for} \quad t_a \leqslant t \leqslant t_r \end{cases} \tag{38}$$

where R_{IDA} is the (numerically determined) drawing radius from the IDA phase ($t_a = 0$ if the IDA phase does not occur).

Once θ assumes θ_r, the CDA phase is over for the following reasons: (1) θ cannot become smaller than θ_r, because the contact angle of a non-moving contact line is bound between θ_r and θ_a; and (2) θ cannot increase again, because this would cause the droplet volume V_d to increase as can be seen from Eq. (2) and $d\xi/d\theta > 0$. Such an increase, however, is not possible due to mass conservation, which requires V_d to decrease, because the liquid volume in the porous medium increases monotonically according to Washburn's equation (8). Thus, the infiltration process is a cascade process, where the CDA phase cannot re-assume the IDA phase, as this would require $\theta \geqslant \theta_a$. Instead, infiltration continues with the DDA phase described next.

2.4. Infiltration during the DDA phase

In the DDA phase, the contact line starts moving again. At any time t, only tubes with radial position $r \leqslant R_d(t)$ participate in the DDA phase. For any time t, we denote the time when infiltration has ended at position r as $t_e(r,t)$. This time t_e is equal to the current time t for tubes with radial position $r \leqslant R_d(t)$ and is smaller than t for tubes with radial position $R_d(t) < r \leqslant R_d(t_a) = R_d(t_r)$, where it is related to the inverse of the unknown variable $R_d(t)$:

$$t_e(r,t) = \begin{cases} t & \text{for} \quad r \leqslant R_d(t) \\ R_d^{-1}(r) & \text{for} \quad R_d(t) < r \leqslant R_d(t_a) \end{cases} \tag{39}$$

The duration, for which infiltration has occurred at time t and position r, is

$$t_i(r,t) = \begin{cases} t_e(r,t) - t_b(r) & \text{for} \quad 0 \leqslant r \leqslant R_d(t_a) \\ 0 & \text{for} \quad r > R_d(t_a) \end{cases} \tag{40}$$

Fig. 5b illustrates t_e and t_i. Using Eqs. (14) and (40), the volume of liquid in the porous medium becomes

$$V_p(t) = 2\pi\epsilon \int_0^{R_d(t_a)} rh(t_e(r,t) - t_b(r))dr \tag{41}$$

Mass conservation according to Eq. (1) together with this expression for V_p and the droplet volume according to Eq. (2) yields

$$2\pi\epsilon \int_0^{R_d(t_a)} rh(t_e(r,t) - t_b(r))dr + R_d^3\xi(\theta) = V_0 \tag{42}$$

Together with Eq. (28) for θ during the DDA phase, Eq. (42) turns into an integro-differential equation for $R_d(t)$:

$$F_r\left(-\frac{\eta\dot{R}_d}{\gamma}, \pi - \theta_r\right) = \pi - \xi^{-1}\left(\frac{1}{R_d^3}\left[V_0 - 2\pi\epsilon\int_0^{R_d(t_a)} rh(t_e(r,t) - t_b(r))dr\right]\right) \tag{43}$$

where $t_e(r)$ is related to $R_d(t)$ through Eq. (39).

The DDA phase is the final phase of infiltration, that is, the cascade of the IDA, CDA, and DDA phases cannot be reversed. After θ starts decreasing from θ_r, two cases may occur. The contact angle θ goes to zero thereby terminating infiltration, because then, according to Eq. (5), the droplet height $H = 0$ and hence the droplet volume $V_d = 0$. Alternatively, θ might increase, $\dot{\theta} \geqslant 0$. The following consideration shows that θ will never exceed θ_r in the latter case, i.e., the motion is always described by the integro-differential equation for the DDA phase. Substituting Eq. (2) into Eq. (1) and differentiating the latter with respect to t yields

$$\dot{V}_p + 3R_d^2\dot{R}_d\xi + R_d^3\frac{d\xi}{d\theta}\dot{\theta} = 0 \tag{44}$$

We can now solve for

$$\dot{\theta} = -\frac{\dot{V}_p + 3R_d^2\dot{R}_d\xi}{R_d^3\frac{d\xi}{d\theta}} \tag{45}$$

As the potential cross-over point to the CDA phase ($\theta = \theta_r$) is approached, the contact line velocity $\dot{R}_d \to 0$, while $d\xi/d\theta > 0$ and $\dot{V}_p > 0$ for $t < \infty$, because liquid volume in any tube of the porous medium increases with time t according to Washburn's equation (8). Hence, $\dot{\theta} < 0$ as the cross-over point is approached. Cross-over would, however, require $\dot{\theta} \geqslant 0$.

2.5. Nondimensional formulation

To minimize the number of parameter dependencies that need to be investigated we nondimensionalize the equations of motion for R_d and θ. We use the radius of the (hypothetically) spherical drop at time $t = 0$ as a typical length scale R_0, i.e., $V_0 = 4\pi R_0^3/3$. A typical velocity can be derived from fluid properties:

$$v_0 = \frac{\gamma}{\eta} \tag{46}$$

We can now introduce a nondimensional time

$$\hat{t} = \frac{v_0}{R_0}t \tag{47}$$

and a nondimensional drawing radius

$$\hat{R}_d(\hat{t}) = \frac{R_d(t)}{R_0} \tag{48}$$

With these definitions we recast the equations of motion, and Eq. (35) for the IDA phase becomes

$$F_a(\hat{R}'_d, \theta_a) = \xi^{-1}\left(\frac{1}{\hat{R}_d^3}\left[\frac{4\pi}{3} - \frac{\pi\Lambda}{\sqrt{8}}\int_0^{\hat{t}} \frac{\hat{R}_d^2(\hat{t} - \hat{\tau})}{\sqrt{\hat{\tau}}}d\hat{\tau}\right]\right) \tag{49}$$

where $\hat{R}'_d = d\hat{R}_d/d\tau$, and

$$\Lambda = \epsilon\sqrt{\frac{R_t}{R_0}\cos\alpha} \tag{50}$$

is a porous permeability parameter that depends on porous medium geometry (through R_t and ϵ), the wetting properties in the porous medium (through α), and initial droplet size (through R_0). Eq. (37) for the CDA phase becomes

$$\theta(\hat{t}) = \xi^{-1}\left(\frac{1}{\hat{R}_d^3(\hat{t}_a)}\left[\frac{4\pi}{3} - \frac{\pi\Lambda}{\sqrt{8}}\int_0^{\hat{t}} \frac{\hat{R}_d^2(\hat{t} - \hat{\tau})}{\sqrt{\hat{\tau}}}d\hat{\tau}\right]\right) \tag{51}$$

Eq. (43) for the DDA phase becomes

$$F_r(-\hat{R}'_d, \pi - \theta_r) = \pi - \xi^{-1}\left(\frac{1}{\hat{R}_d^3}\left[\frac{4\pi}{3} - \pi\Lambda\sqrt{2}\int_0^{\hat{R}_d(\hat{t}_a)} \hat{r}\sqrt{\hat{t}_e(\hat{r},\hat{t}) - \hat{t}_b(\hat{r})}d\hat{r}\right]\right) \tag{52}$$

where $\hat{r} = r/R_0$, $\hat{t}_b = t_b v_0/R_0$, and $\hat{t}_e = t_e v_0/R_0$. If an infiltration event starts out with the IDA or DDA phase, the initial condition is

$$\hat{R}_d(0) = \left(\frac{4\pi}{3\xi(\theta_i)}\right)^{1/3} \tag{53}$$

If it starts with the CDA phase, the initial condition is $\theta(0) = \theta_i$.

We identify the following four nondimensional parameters that govern the infiltration problem:

1. The initial contact angle of the drop, θ_i;
2. The equilibrium advancing contact angle of the drop, θ_a;
3. The equilibrium receding contact angle of the drop, θ_r; and
4. The porous permeability parameter Λ.

In addition, one needs to specify two models for dynamic contact angle, F_a and F_r. Lacking a generally accepted model F for dynamic contact angle θ on porous surfaces, the simulations used to investigate general properties of our theoretical model (see Sections 3–5) employ Eq. (20) to parameterize both F_a and F_r. Only in the case study (see Section 6) and in a comparison to an analytical solution (see Appendix A), we use Eq. (21) and consider c_t to be a fit parameter.

Please see Appendix A for the numerical methods used to solve the nondimensional equations of motion. In Appendix A, we also present comparisons of numerical simulations to analytical solutions that serve as a validation of the numerical solution techniques.

3. Sequences of infiltration phases

Depending on the initial contact angle of the droplet, θ_i, an infiltration event starts out with either the IDA, CDA, or DDA phase. The following subsections will treat these three cases as well as the possible sequences of infiltration phases that may occur. To generate these cases we performed a set of simulations that use different values for θ_i, θ_a, and θ_r but keep Λ from Eq. (50) constant. The value of θ_i relative to θ_a and θ_r determines with which phase infiltration starts. The final phase is determined by the exact values of θ_a, θ_r, and Λ. If the DDA phase is assumed, infiltration is over either once the drawing radius R_d becomes smaller than the radius of the porous medium tubes, R_t, according to Eq. (15) or once the contact angle of the droplet $\theta = 0$, which implies that the droplet height $H = 0$ according to Eq. (5).

3.1. Infiltration starts with the IDA phase, $\theta_i > \theta_a$

Four different cases concerning the subsequent occurrence of the CDA and DDA phases exist (see Fig. 6):

(a) Droplet infiltration includes the DDA phase. Infiltration is over when $R_d(t_f) = R_t$, whereas the contact angle of the droplet remains positive throughout the entire infiltration, $\theta(t) > 0$ for $0 \leqslant t \leqslant t_f$.
(b) Droplet infiltration includes the DDA phase. Infiltration is over when $\theta(t_f) = 0$, whereas $R_d(t) > R_t$ for $0 \leqslant t \leqslant t_f$.
(c) If $\theta_r = 0$, then the DDA phase does not occur.
(d) If $\theta_a = 0$, then the CDA and DDA phases do not occur. This case has been investigated by Holman et al. (2002).

Fig. 6a illustrates that there is a tendency of the contact angle θ to rebound to θ_r during the final DDA phase, that is, to increase after the initial decrease. Only if θ_r is close to 0 and if the lengths of the liquid slugs in the tubes, h, are sufficiently small, then, once the DDA phase is assumed, the liquid will be sucked into the tubes quickly enough such that a sufficiently large contact line velocity $\dot{R}_d$ can be achieved that allows for $\theta(t_f) = 0$. This is the case for the simulation shown in Fig. 6b, whereas the simulation shown in Fig. 6a ends with $\theta(t_f) > 0$ and $R_d(t_f) = R_t$ because of the larger θ_r. The values of θ_i and θ_a also control whether $\theta(t_f) = 0$ or $\theta(t_f) > 0$, because they control the drawing area and hence the length of the liquid slugs at the beginning of the DDA phase. For smaller θ_i values, the droplet is flatter (for a fixed initial droplet volume, $\Lambda = \text{const.}$); hence, the liquid slugs at the beginning of the DDA are shorter, and it is more likely that $\theta(t_f) = 0$. The total time of infiltration tends to be shorter for lower θ_r values, because the drawing area in the DDA phase becomes larger as is evident when comparing Fig. 6a and b.

3.2. Infiltration starts with the CDA phase, $\theta_a \geqslant \theta_i > \theta_r$

To categorize infiltration events that begin with the CDA phase, we can build on the analysis performed for the case where infiltration starts out with the IDA phase and simply remove the IDA phases in Fig. 6. Fig. 7 shows the three cases that may occur:

(a) Droplet infiltration includes the DDA phase. Infiltration is over, when the drawing radius becomes smaller than the size of the porous medium tubes, $R_d(t_f) = R_t$, whereas $\theta(t) > 0$ for $0 \leqslant t \leqslant t_f$.
(b) Droplet infiltration includes the DDA phase. Infiltration is over, when the contact angle of the droplet vanishes, $\theta(t_f) = 0$, whereas $R_d(t) > R_t$ for $0 \leqslant t \leqslant t_f$. As compared to Case (a), the lower θ_r value allows for $\theta(t_f) = 0$ at the end of the DDA phase.
(c) If $\theta_r = 0$, then the DDA phase does not occur. This case has been investigated by Denesuk et al. (1993).

3.3. Infiltration starts with the DDA phase, $\theta_r \geqslant \theta_i$

To categorize infiltration events that start out with the DDA phase, we can build on the analysis performed for the case where infiltration starts out with the CDA phase and simply remove the CDA phases in Fig. 7. Fig. 8 shows the two cases that may then occur:

(a) Infiltration is over, when the drawing radius becomes smaller than the size of the porous medium tubes, $R_d(t_f) = R_t$, whereas $\theta(t) > 0$ for $0 \leqslant t \leqslant t_f$. At the very end of the simulation, for times to the right of the dashed lines in Fig. 8a, Inequality (17) is not fulfilled. Hence, the model underestimates the rate of infiltration.
(b) Infiltration is over, when the contact angle of the drop vanishes, $\theta(t_f) = 0$, whereas $R_d(t) > R_t$ for $0 \leqslant t \leqslant t_f$. Again, the lower θ_r value allows for $\theta(t_f) = 0$.

4. Sensitivity to porous permeability parameter Λ

In the previous section, we discussed the effects of three out of the four nondimensional parameters that govern droplet infiltration. Let us finally discuss the role of Λ defined in Eq. (50). We consider a scenario where θ_i, θ_r, and θ_a are being held constant while Λ is decreased.

As Λ decreases, infiltration slows down. A decrease in Λ can be accomplished by a change of several dimensional quantities: A decrease in tube size R_t will increase viscous dissipation in the liquid and hence slow down flow. A decrease in porosity ϵ will reduce the amount of pore space available for liquid withdrawal and hence also slow down infiltration. An increase in tube contact angle α (up to the maximum value of 90°) will reduce the capillary pressure at the advancing liquid–air interface and hence the driving pressure gradient in the liquid. The two simulations presented in Fig. 9 show that lowering Λ slows down infiltration in nondimensional temporal space. This statement is also correct in dimensional temporal space as the relationship between t and $\hat{t}$ according to Eq. (47) does not change as one varies R_t, ϵ, and α. Increasing the initial droplet size R_0 also causes Λ to decrease and hence infiltration to slow down, both in nondimensional and dimensional temporal space (even though the relationship between t and $\hat{t}$ depends on R_0), because a larger droplet volume requires a longer time of infiltration.

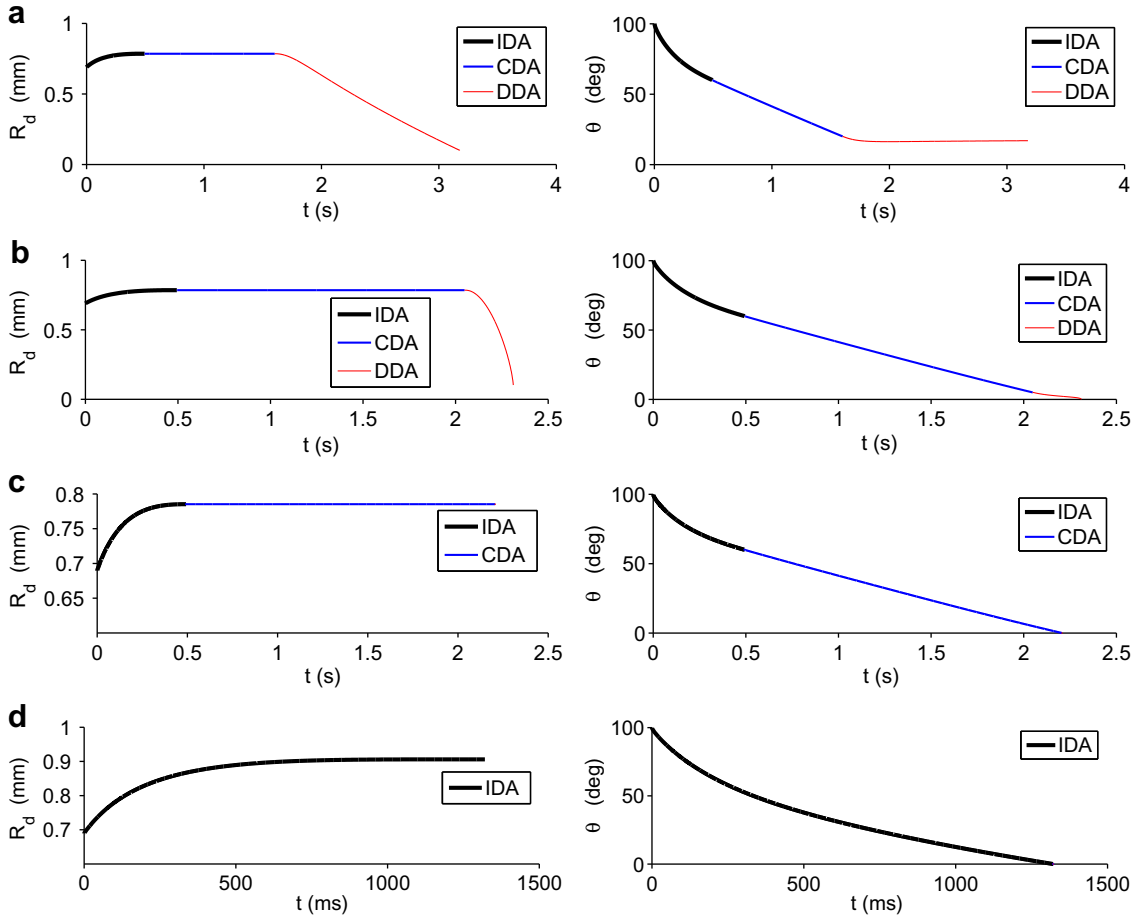

Fig. 6. The four cases that may occur, if the IDA phase is assumed. (a) For $\theta_i = 100°$, $\theta_a = 60°$, $\theta_r = 20°$, infiltration ends in the DDA phase when $R_d = R_t$. (b) For $\theta_i = 100°$, $\theta_a = 60°$, $\theta_r = 5°$, infiltration ends in the DDA phase when $\theta = 0°$. (c) For $\theta_i = 100°$, $\theta_a = 60°$, $\theta_r = 0°$, infiltration ends in the CDA phase. (d) For $\theta_i = 100°$, $\theta_a = 0°$, infiltration ends in the IDA phase. Other simulation parameters: $R_t = 0.1$ mm, $R_0 = 0.6$ mm, $\alpha = 0°$, $\epsilon = 0.3$, fluid properties of silicone oil.

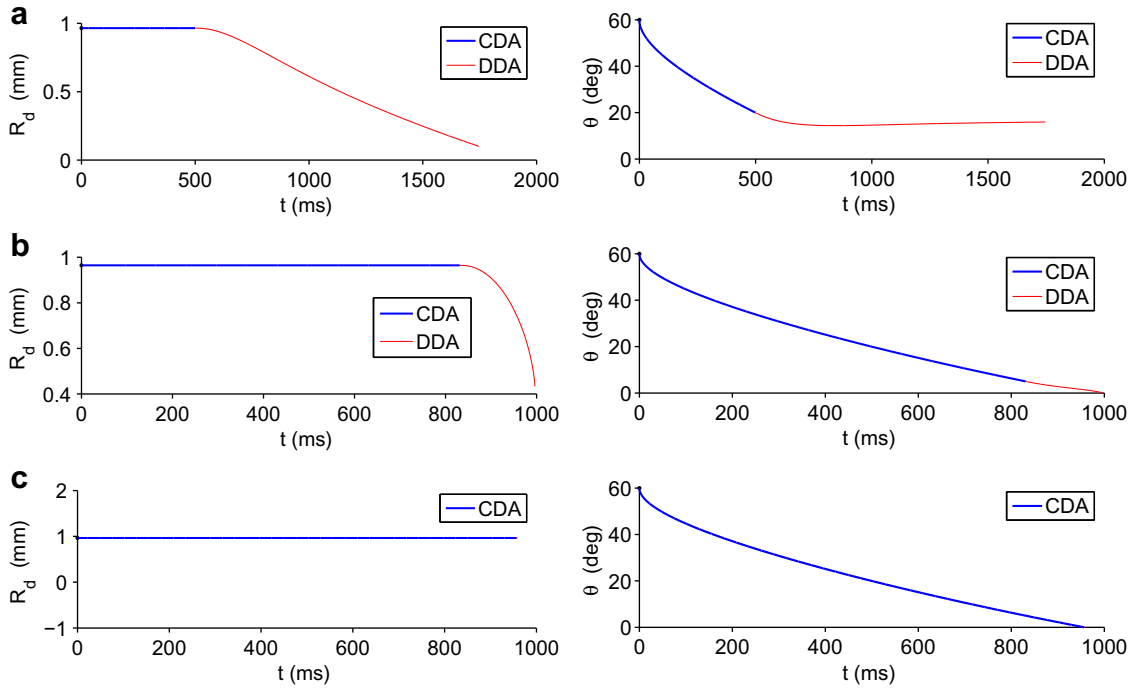

Fig. 7. The three cases that may occur, if infiltration starts with the CDA phase. (a) For $\theta_i = \theta_a = 60°$, $\theta_r = 20°$, infiltration ends in the DDA phase when $R_d = R_t$. (b) For $\theta_i = \theta_a = 60°$, $\theta_r = 5°$, infiltration ends in the DDA phase when $\theta = 0°$. (c) For $\theta_i = \theta_a = 60°$, $\theta_r = 0°$, infiltration ends during the CDA phase because $\theta_r = 0°$. Other simulation parameters: $R_t = 0.1$ mm, $R_0 = 0.6$ mm, $\alpha = 0°$, $\epsilon = 0.3$, fluid properties of silicone oil.

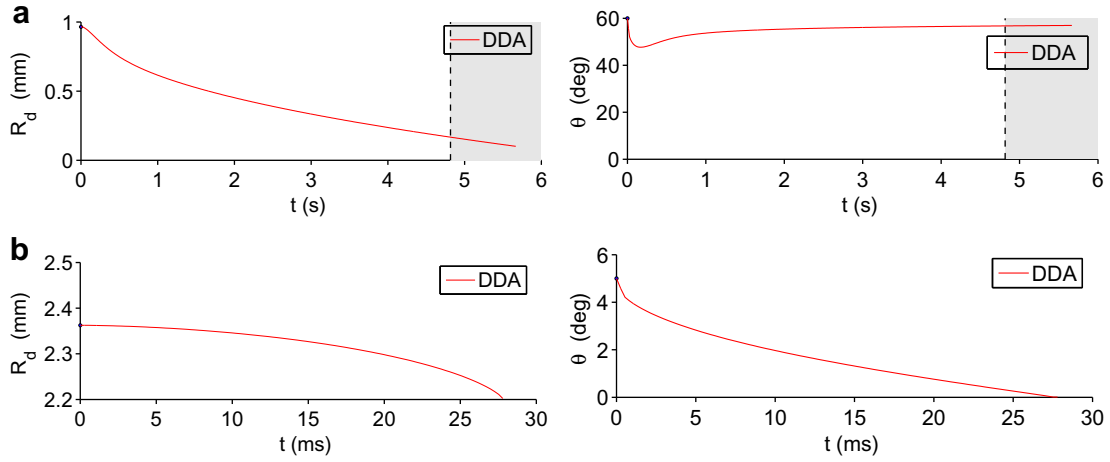

Fig. 8. The two cases that may occur, if infiltration starts with the DDA phase. (a) For $\theta_i = \theta_r = 60°$, infiltration ends when $R_d = R_t$. (b) For $\theta_i = \theta_r = 5°$, infiltration ends when $\theta = 0°$. Other simulation parameters: $R_t = 0.1$ mm, $R_0 = 0.6$ mm, $\alpha = 0°$, $\epsilon = 0.3$, fluid properties of silicone oil.

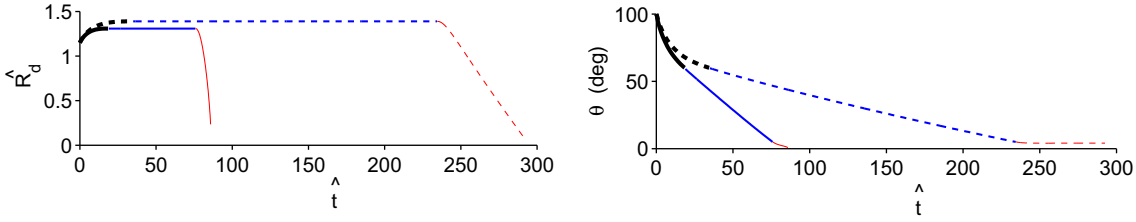

Fig. 9. Sensitivity of infiltration to the porous permeability parameter Λ. Solid lines: $\Lambda = 0.12$. Dashed lines: $\Lambda = 0.06$. Other simulation parameters: $\theta_i = 100°$, $\theta_a = 60°$, and $\theta_r = 5°$. Color code as in Figs. 6–8. (For interpretation of the references to color in this figure legend, the reader is referred to the web version of this article.)

As illustrated in Fig. 9, a smaller Λ value also makes $\theta(t_f) = 0°$ less likely, because the stronger flow resistance prevents the droplet from achieving the high contact line velocity $\dot{R}_d$ associated with $\theta = 0°$.

5. ODE approaches for the IDA and DDA phases

5.1. Motivation

In our theory, the dynamics of the IDA and DDA phases is governed by the integro-differential equations (35) and (43). This is because the state of our droplet–porous medium system is not only described by the instantaneous values of R_d and θ but also by the history of the system, that is, the order in which the porous medium tubes have been invaded by liquid. Many scientific computing packages, however, do not provide numerical solvers for integro-differential equations. Hence, we developed approaches that approximate the integro-differential equations by ordinary differential equations (ODEs), for which a wealth of numerical solvers exists.

5.2. IDA phase

Deriving Eq. (34) with respect to time t and using Eq. (27) for θ and Eq. (6) for $d\xi/d\theta$, we obtain

$$3\xi(\theta)R_d^2\dot{R}_d + \frac{\pi}{(1+\cos\theta)^2}\frac{dF_a}{d\hat{v}}\frac{\eta}{\gamma}\ddot{R}_d R_d^3 + \frac{\pi A\epsilon}{2}\frac{d}{dt}\int_0^t \frac{R_d^2(t-\tau)}{\sqrt{\tau}}d\tau = 0 \tag{54}$$

This is an integro-differential equation for $R_d(t)$, where $R_d(0)$ and $\dot{R}_d(0)$ are the initial conditions. To turn Eq. (54) into an ODE we turn the derivative of the integral into a function of R_d and its derivatives. For that, we expand the well-behaved R_d^2 in the integrand in a Taylor series: $R_d^2(t-\tau) \approx R_d^2(0) + 2\dot{R}_d(0)R_d(0)(t-\tau)$. Hence, we can evaluate the derivative of the integral in Eq. (54),

$$\frac{d}{dt}\int_0^t \frac{R_d^2(t-\tau)}{\sqrt{\tau}}d\tau \approx \frac{R_d^2(0)}{\sqrt{t}} + 4\sqrt{t}R_d(0)\dot{R}_d(0) \tag{55}$$

Finally, substituting the latter equation into Eq. (54) yields an ODE for $R_d(t)$:

$$0 = 3\xi(\theta)R_d^2(t)\dot{R}_d(t) + \frac{\pi}{(1+\cos\theta)^2}\frac{dF_a}{d\hat{v}}\frac{\eta}{\gamma}\ddot{R}_d(t)R_d^3(t) + \frac{\pi A\epsilon}{2}\left[\frac{R_d^2(0)}{\sqrt{t}} + 4\sqrt{t}R_d(0)\dot{R}_d(0)\right] \tag{56}$$

To facilitate the numerical solution, we nondimensionalize this second-order ODE and recast it as a system of two first-order ODEs where $\hat{y}_1(\hat{t}) = R_0 R_d(t)$ and $\hat{y}_2(\hat{t}) = v_0\dot{R}_d(t)$:

$$\begin{pmatrix}\hat{y}_1' \\ \hat{y}_2'\end{pmatrix} = \begin{pmatrix}\hat{y}_2 \\ -\frac{3\xi\hat{y}_1^2\hat{y}_2 + \frac{\pi A}{\sqrt{8}}\left(\frac{\hat{y}_1^2(0)}{\sqrt{\hat{t}}} + 4\sqrt{\hat{t}}\hat{y}_1(0)\hat{y}_2(0)\right)}{\frac{\pi}{(1+\cos\theta)^2}\frac{dF}{d\hat{v}}\hat{y}_1^3}\end{pmatrix} \tag{57}$$

We used the Runge–Kutta method (Press et al., 1992) to solve this ODE system. Fig. 10 compares the prediction from solving the integro-differential equation (35) to the one from solving the ODE. The agreement is excellent for small values of t and is good for most of the IDA phase. The deviation between the two predictions increases with time t, because then the Taylor series expansion for R_d^2 becomes less accurate.

5.3. DDA phase

One can describe infiltration by an ODE, if infiltration does not involve the IDA phase (or if the duration of the IDA phase is negli-

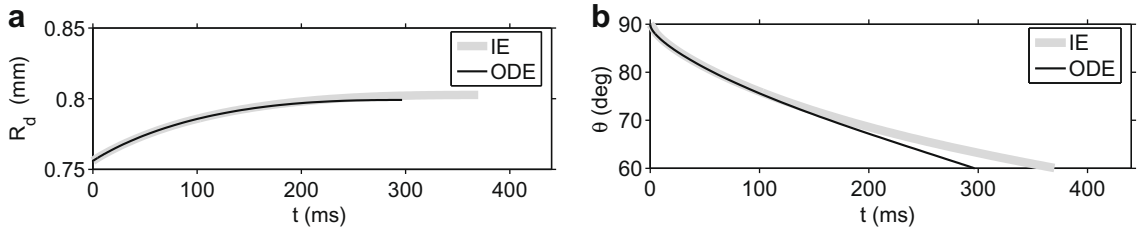

Fig. 10. Comparison of the integro-differential equation approach for the IDA phase to the ODE approach. Simulation parameters: $\theta_i = 90°$, $\theta_a = 60°$, $R_t = 0.1$ mm, $R_0 = 0.6$ mm, $\epsilon = 0.3$, $\alpha = 0°$, fluid properties of silicone oil.

gible). Infiltration may, however, include the CDA phase. Figs. 7a,b and 8 show examples for such scenarios. We start from Eq. (42) using $t_b(r) = 0$ for $r \leqslant R_d(0)$:

$$2\pi\epsilon \int_0^{R_d(0)} rh(t_e(r,t))dr + R_d^3\xi(\theta) = V_0 \tag{58}$$

where θ is given by Eq. (28). We recast the integral by using $h(t_e(r,t)) = \int_0^{t_e(r,t)} \dot{h}(\tau)d\tau$ and $\dot{h}(\tau) = A/(2\sqrt{\tau})$:

$$\pi\epsilon A \int_0^{R_d(0)} r \int_0^{t_e(r,t)} \frac{1}{\sqrt{\tau}} d\tau dr + R_d^3\xi(\theta) = V_0 \tag{59}$$

Changing the order of integration yields

$$\frac{\pi\epsilon A}{2} \int_0^{t} \frac{R_d^2(\tau)}{\sqrt{\tau}} d\tau + R_d^3\xi(\theta) = V_0 \tag{60}$$

Differentiation with respect to t and using Eqs. (6) and (28) yields an ODE for $R_d(t)$:

$$\frac{\pi\epsilon A}{2}\frac{R_d^2(t)}{\sqrt{t}} + 3R_d^2\dot{R}_d\xi(\theta) + R_d^3\frac{\pi}{(1+\cos\theta)^2}\frac{dF_r(\hat{v},\pi-\theta_r)}{d\hat{v}}\frac{\eta}{\gamma}\ddot{R}_d = 0 \tag{61}$$

where $\hat{v} = -\eta\dot{R}_d/\gamma$ according to Eq. (19). We obtain

$$\frac{dF_r}{d\hat{v}} = 4.96 \cdot 0.702 \cdot \hat{v}^{-0.298}\frac{1-\cos\theta_0}{\sin\theta}\operatorname{sech}^2(4.96 \cdot \hat{v}^{0.702}) \tag{62}$$

for a dynamic contact angle according to Eq. (20) and

$$\frac{dF_r}{d\hat{v}} = \frac{c_t}{3(\pi-\theta)^2} \tag{63}$$

for a dynamic contact angle according to Eq. (21). The initial conditions for Eq. (61) are given by $R_d(t_r)$ and $\dot{R}_d(t_r)$.

To facilitate the numerical solution of the second-order ODE (61), we nondimensionalize it and recast it as a system of two first-order ODEs:

$$\begin{pmatrix}\hat{y}_1' \\ \hat{y}_2'\end{pmatrix} = \begin{pmatrix}\hat{y}_2 \\ -\left(\frac{dF_r}{d\hat{v}}\right)^{-1}\frac{1}{\hat{y}_1}\left(\frac{\Lambda}{\sqrt{8}}\frac{(1+\cos\theta)^2}{\sqrt{\hat{t}}} + \sin\theta(2+\cos\theta)\hat{y}_2\right)\end{pmatrix} \tag{64}$$

where $\hat{y}_1(\hat{t}) = R_0R_d(t)$, $\hat{y}_2(\hat{t}) = v_0\dot{R}_d(t)$, and where we used Eq. (3) for $\xi(\theta)$. We use the Runge–Kutta method to solve this ODE. Special caution has to be taken, however, if (1) the DDA phase starts out with the receding contact angle θ_r and the Jiang et al. (1979) model for dynamic contact angle according to Eq. (20) is used because then $dF_r/d\hat{v} = \infty$ for $\hat{v}(0) = 0$ according to Eq. (24) and/or (2) the entire infiltration event starts out with the DDA phase because then $1/\sqrt{\hat{t}} = \infty$ for $t = t_r = 0$. In both cases, we use the following algorithm for the first time step $\Delta\hat{t}$ of the DDA phase, which starts out with $\hat{y}_2 \approx 0$ and $\hat{y}_1(\hat{t}) \approx \hat{y}_1(\hat{t}_a)$. Using the second row of Eq. (64), $d\hat{v} = -d\hat{y}_2$, and $d\theta = -dF_r$, we can solve for the change in contact angle:

$$d\theta = -\frac{1}{\hat{y}_1(\hat{t}_a)}\left(\frac{\Lambda}{\sqrt{8}}\frac{(1+\cos\theta)^2}{\sqrt{\hat{t}}} + \sin\theta(2+\cos\theta)\hat{y}_2(\hat{t}_a)\right)d\hat{t} \tag{65}$$

Integration over the initial time step Δt yields:

$$\Delta\theta = \theta(\hat{t}_a+\Delta\hat{t}) - \theta(\hat{t}_a) = -\frac{1}{\hat{y}_1(\hat{t}_a)} \times \left[\frac{\Lambda}{\sqrt{2}}(1+\cos\theta)^2 \times \left(\sqrt{\hat{t}_a+\Delta\hat{t}} - \sqrt{\hat{t}_a}\right) + \sin\theta(2+\cos\theta)\hat{y}_2(\hat{t}_a)\Delta\hat{t}\right] \tag{66}$$

From $\Delta\theta$, we can now calculate the contact line velocity according to Eq. (28):

$$-\hat{R}'(\hat{t}_a+\Delta\hat{t}) = F_r^{-1}(\pi-\theta_a-\Delta\theta,\pi-\theta_r) \tag{67}$$

From time $\hat{t}_a + \Delta\hat{t}$ on, Eq. (64) can be solved numerically with initial drawing radius $\hat{R}_d(\hat{t}_a+\Delta\hat{t}) \approx \hat{R}_d(\hat{t}_a)$ and initial contact line velocity $\hat{R}_{d'}(\hat{t}_a+\Delta\hat{t})$. Only if one uses the modified first time step, the simulated $\hat{R}_d$ and $\hat{R}_{d'}$ values are continuous at $\hat{t} = \Delta\hat{t}$.

Fig. 11 shows excellent agreement between the numerical solution of the ODE (64) and the numerical solution of the integro-differential equation (43). This fact can be considered as a validation of the numerical implementations of both the ODE and integro-differential equation.

6. Case study

We tested our model by comparing it to an experiment performed by Clarke et al. (2002) where a droplet infiltrated into a frit with a nominal pore diameter of 0.22 μm. Clarke et al. (2002) fitted their infiltration model to their data and obtained a fit which indicates potential shortcomings of their modeling approach. Fig. 12 shows that the slopes of both R_d and θ at the final measurement time are not described well by the model, perhaps because Clarke et al. (2002) assumed the CDA phase not to occur, $\theta_a = \theta_r$, for that data set.

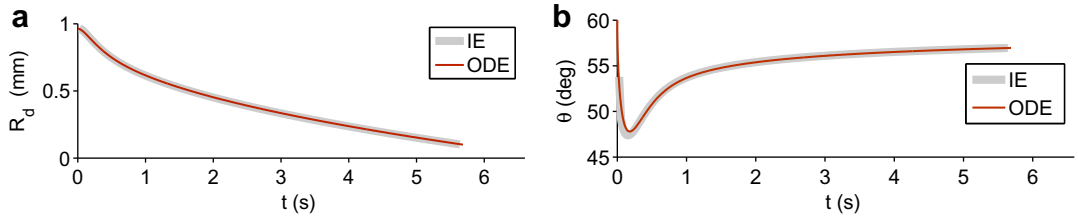

Fig. 11. Comparison of the integro-differential equation approach for the DDA phase to the ODE approach. Simulation parameters: $\theta_i = \theta_r = 60°$, $R_t = 0.1$ mm, $R_0 = 0.6$ mm, $\alpha = 0°$, and liquid properties of silicone oil.

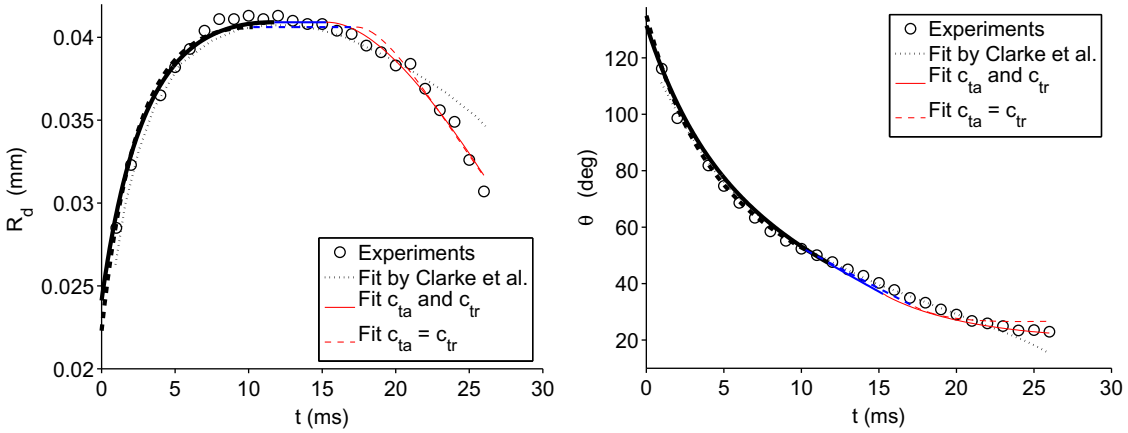

Fig. 12. Model fits to experimental data by Clarke et al. (2002). Our model fits match the data better than the model fit by Clarke et al. (2002), because we account for the CDA phase and allow for different parameterizations of dynamic contact angle in the IDA and DDA phases. Color code as in Figs. 6–8. (For interpretation of the references to color in this figure legend, the reader is referred to the web version of this article.)

Using two different sets of fit parameters, we fitted our model to that data set by minimizing the deviation between measured and simulated $R_d(t)$ and $\theta(t)$ curves. Both sets use R_0, $v_0 = \gamma/\eta$, θ_i, θ_a, θ_r, and Λ as fit parameters, but the sets differ in the parameterization of dynamic contact angle. Contrary to Clarke et al. (2002), we allow the CDA phase to occur. We use the model for dynamic contact angle according to Eq. (21), where we consider c_t to be a fit parameter in order to account for the presence of a permeable solid surface. Our first fit allows for different parameterizations of the dynamic contact angle model for the IDA and DDA phases by using different c_t values labeled as c_{ta}, and c_{tr}, respectively. We obtain $c_{ta} = 814$ and $c_{tr} = 1479$. Fig. 12 shows that our model describes the data much better than the fit by Clarke et al. (2002). In our second fit, we use the same parameterization for F_a and F_r for the IDA and DDA phases and obtain $c_{ta} = c_{tr} = 1073$. As shown in Fig. 12, the quality of the fit becomes worse but is still better than the fit by Clarke et al. (2002). A comparison of the three fits suggests that (1) it is important to account for contact angle hysteresis and the resulting physical process of the CDA phase; and (2) the law for dynamic contact angle is different for the IDA and DDA phases. The significant difference between c_{ta} and c_{tr} is not unexpected, because liquid displaces air during the IDA phase, while air displaces liquid during the DDA phase. Cox' (1986) theory then suggests that F_a differs significantly from F_r because of the dramatic difference in the viscosity ratio.

The fitted values for c_{ta} and c_{tr} are significantly higher than the value obtained for impermeable surfaces, $c_t \approx 72$. Since $\theta^3 - \theta_0^3$ follows the general trend of the uncompensated Young force on the contact line, $\gamma(\cos\theta_0 - \cos\theta)$ (de Gennes et al., 1990), we can conclude that the uncompensated Young force is higher for permeable than for impermeable surfaces for a fixed contact line velocity $\dot{R}_d$. The uncompensated Young force is countered by viscous forces in the vicinity of the contact line (Leger and Joanny, 1992). Hence, the larger c_t values are reasonable, because viscous forces increase with surface roughness.

7. Conclusions and discussion

We developed a model for infiltration of droplets into porous media that accounts for a dynamic contact angle θ of the droplet as well as hysteresis of the equilibrium contact angle. As a result, droplet infiltration may involve an IDA, CDA, and DDA phase, which may occur only in this order; however, the entire process may start and end in any of the three phases. Our theory agrees very well with an experiment performed by Clarke et al. (2002) as illustrated in Fig. 12 and, as required, converges to analytical solutions for the CDA and DDA phases as shown in Appendix A. Fig. 13 summarizes the six different sequences that may occur. The behavior of contact angle θ critically affects the duration of the three infiltration phases and the total time of infiltration. In the nine simulations presented in Figs. 6–8, we kept the initial droplet volume, the porous medium properties, and the liquid properties constant, while varying θ_i, θ_a, and θ_r. The total time of infiltration may vary by several orders of magnitude. Smaller θ_r values tend to shorten the total time of infiltration. Even if the initial drawing radius, $R_d(0)$, and hence θ_i, are the same, the total

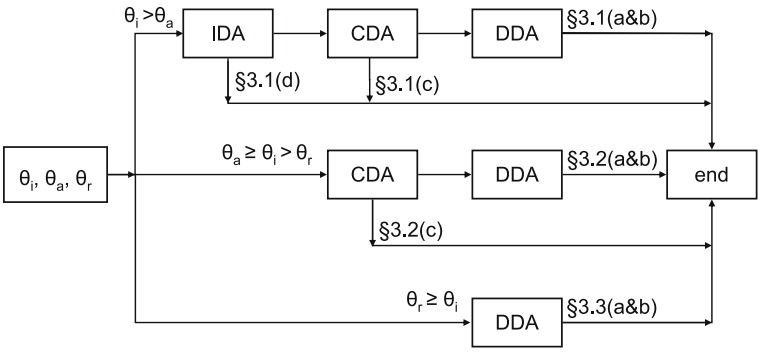

Fig. 13. Overview of the six sequences of IDA, CDA, and DDA phases that may occur. The initial contact angle θ_i determines with which phase infiltration begins. Infiltration then follows a cascade that may include the IDA, CDA, and DDA phases. Infiltration may end in any of the three phases. Labels at the arrows toward the end box denote the sections (and case labels) that discuss the corresponding sequences.

time of infiltration may vary by a factor of 2.5, as can be seen from a comparison of Fig. 6a and d. Likewise, θ_i, θ_a, and θ_r affect the dependence of drawing radius R_d on time t. This may be of crucial interest when liquid droplets are administered either intentionally or unintentionally to porous surfaces.

The porous permeability parameter Λ defined in Eq. (50) significantly affects the time of infiltration. Increasing liquid viscosity η and lowering interfacial tension γ increases the total time of infiltration. Note that the four nondimensional parameters that formulate the problem do not depend on these two quantities. An increase in infiltration time occurs, because η and γ affect the typical velocity v_0, which in turn affects the relation between dimensional and nondimensional time according to Eq. (47).

In general, the dynamics of the IDA and DDA phases are given by integro-differential equations, because the liquid distribution in the porous medium tubes memorizes an infiltration event in a way not solely captured by the state variables R_d and θ. One can refer to this phenomenon as hysteresis. Denesuk et al. (1993) were able to turn an integro-differential for droplet infiltration into an ODE, because they considered infiltration events, in which all tubes underneath the droplet are invaded by liquid at time $t = 0$. This condition, however, is not met in the IDA phase. Nonetheless, we were able to approximate the early stage of the IDA phase by the ODE given by Eq. (56). If infiltration starts out with the CDA or DDA phase, infiltration can be described exactly by the ODE given by Eq. (61). Contrary to the ODE derived by Denesuk et al. (1993), our ODE accounts for a dynamic contact angle θ. ODE approaches have the advantage that they can be solved numerically with many scientific computing packages. In this work, they also served as an additional means of validating our numerical method for solving the integro-differential equations.

Even though the functional form F for the dynamic contact angle θ given by Eq. (18) is quite general, little is known about how F exactly depends on nondimensional contact line velocity $\hat{v}$. In this paper, we used expressions for F that are based on measurements in capillary tubes with impermeable walls. We expect an F relation for a porous surface to differ significantly from the one for an impermeable surface, even if the solid phase consists of the same material, because the surface of a porous medium is much more irregular and because liquid loss through infiltration into the porous medium changes flow boundary conditions. Indeed when fitting Eq. (21) for F, which has been obtained for impermeable surfaces, to an infiltration experiment, we obtain higher c_t values (see Section 6). This suggests that a highly irregular permeable surface causes a higher nonequilibrium force on the moving contact line of a droplet than a relatively smooth impermeable surface. More studies are, however, needed to confirm and potentially revise our functional form for F on permeable surfaces.

Using different models for dynamic contact angle θ will not change our main findings: (1) The order in which the infiltration phases occur, (2) the dimensional analysis, and (3) the approximation of the equations of motion by ODEs. This is because our analyses only employ a very general and reasonable property of dynamic contact angle θ, namely that θ increases monotonically with the contact line velocity $\hat{v}$.

Our theory is based on several simplifying assumptions which might need to be reconsidered in certain applications:

1. Our theory does not explicitly model flow within the droplet. It assumes uniform pressure in the droplet. This assumption may not be appropriate for infiltration of a droplet falling down onto a porous surface immediately after the impact, because then the droplet shape and pressure distribution in the droplet may be very complicated due to the internal flows induced by the impact.
2. While we accounted for a dynamic droplet contact angle θ, we did not account for a dynamic tube contact angle α. Even though this is not entirely consistent, the occurrence of the IDA, CDA, and DDA phases were our prime interest. Principally, it is possible to account for a dynamic contact angle in the tubes. Chebbi (2007), for example, extended Washburn's theory to account for the dynamic contact angle law given by Eq. (20); however, the resulting approximate analytical solutions are only valid for small or large times. This causes problems with the implementation of these solutions. We expect our simulation results to change, if a dynamic α was accounted for; however, we do not expect the main conclusions of the paper to change.
3. One can easily envision scenarios (e.g., large rain drops falling onto soil), where one cannot use the spherical cap approximation for droplet shape due to gravity.
4. Our model assumes the porous medium to consist of tubes that are not interconnected. The pore spaces of many porous media possess, however, a much more complicated topology, which will cause lateral spreading of the liquid in the porous medium. Future work should account for the network structure of porous media. For that one could build on the theories for droplet infiltration developed by Anderson (2005) and Daniel et al. (2006).

Acknowledgments

This work was supported by the US Army under Contract No. W91ZLK-06-P-1058. We thank Mark Robbins for useful discussions and Andrew Clarke for providing us with his experimental data (Clarke et al., 2002) in electronic format.

Appendix A. Numerical solution

A.1. IDA phase

The integro-differential equation for the IDA phase given by Eq. (49) is of the following form:

$$R' = \mathscr{H}(R(t), I(t)) \tag{68}$$

where we omitted the subscript d in $\hat{R}_d$ as well as the hats used to indicate nondimensional variables,

$$I(t) = \int_0^t \frac{R^2(t-\tau)}{\sqrt{\tau}} d\tau \tag{69}$$

and

$$\mathscr{H}(R, I) = F_a^{-1}\left(\xi^{-1}\left(\frac{1}{R^3}\left[\frac{4\pi}{3} - \frac{\pi\Lambda}{\sqrt{8}} I\right]\right), \theta_a\right) \tag{70}$$

Note that $F_a^{-1}(\xi^{-1})$ is a (unique) function, because both F_a and ξ are monotonically increasing functions. We invert ξ numerically using a linear interpolation on a discrete set of $\xi_n = \xi(\theta_n)$ values evaluated for a dense set of θ_n values ranging from 0 to π. The F_a functions can also be inverted numerically. In this paper, however, we used Eqs. (20) and (21) for F_a. Hence, we could simply use the closed-form expression for F_a^{-1} given by Eqs. (23) and (25). Eq. (68) allows using the numerical-solution technique described in Chapter 11 of Linz (1985). We discretize time,

$$t_n = n\Delta t \tag{71}$$

where $n = 0, 1, 2, \ldots$ and Δt is the time step. Then,

$$R_n = R(t_n) \tag{72}$$

The integral deserves special attention, because the singularity in the integrand at $\tau = 0$ causes a problem when using the trapezoidal integration rule. Hence, the integral is split up into two parts:

$$I_n = I(t_n) = \underbrace{\int_0^{\Delta t} \frac{R^2(t_n-\tau)}{\sqrt{\tau}}d\tau}_{I_A} + \underbrace{\int_{\Delta t}^{t_n} \frac{R^2(t_n-\tau)}{\sqrt{\tau}}d\tau}_{I_B} \quad (73)$$

To determine I_A, we expand R^2 in a first-order Taylor series, $R^2(t_n-\tau) \approx R_n^2 - 2R_nR_{n'}\tau$, where $R'_n = (R_n - R_{n-1})/\Delta t$. With that

$$I_A = 2R_n^2(\Delta t)^{1/2} - \frac{4}{3}R_nR_{n'}(\Delta t)^{3/2} \quad (74)$$

For I_B, we employed the trapezoidal rule. To step forward in time, we integrate Eq. (68):

$$\int_{t_n}^{t_{n+1}} R'dt = R_{n+1} - R_n = \int_{t_n}^{t_{n+1}} \mathscr{H}(R(t), I(t))dt \quad (75)$$

Approximating the integral with the trapezoidal rule yields

$$R_{n+1} = R_n + [\mathscr{H}(R_{n+1}, I_{n+1}) + \mathscr{H}(R_n, I_n)]\frac{\Delta t}{2} \quad (76)$$

This is a nonlinear equation for R_{n+1} that is in standard form for solution with the method of fixed-point (Picard) iteration (Press et al., 1992). We terminate the iteration when $|R_{n+1}^{i+1} - R_{n+1}^{i}|/R_{n+1}^{i+1}$ is smaller than a prescribed error, e.g., 10^{-6}, where the superscript denotes the iteration number. In convergence studies, we ensured that simulation results are not sensitive to the termination threshold.

A.2. CDA phase

To solve Eq. (51) numerically we first determine t_r, that is, the time when the CDA phase is over. For that, we evaluate Eq. (51) for an initial guess for t_r and iterate t_r until $\theta(t_r) = \theta_r$. Then, we calculate θ at discrete times t_n between t_a and t_r according to Eq. (51). We evaluate the time integral in Eq. (51) according to Eq. (73) for the IDA phase, where we use the same time steps for the IDA and CDA phases. By employing the same time steps, the R_d^2 and $\sqrt{\tau}$ terms can be evaluated at the same t_n values when numerically evaluating the integral, thus avoiding interpolating either variable.

A.3. DDA phase

The integro-differential equation for the DDA phase, Eq. (52), is of the form given by Eq. (68), but $I(t)$ is now given by

$$I(t) = \int_0^{R_d(t_a)} r\sqrt{t_e(r,t) - t_b(r)}dr \quad (77)$$

and

$$-\mathscr{H}(R,I) = F_r^{-1}\left(\pi - \xi^{-1}\left(\frac{1}{R^3}\left[\frac{4\pi}{3} - \pi\Lambda\sqrt{2}I\right]\right), \pi - \theta_r\right) \quad (78)$$

As in the IDA phase, we discretize time, $t_n = t_r + n\Delta t$, and integrate Eq. (68) from t_n to t_{n+1} to obtain Eq. (76), which again can be solved by the method of Picard iteration. Only the function $\mathscr{H}$ and the integral I are defined differently. We used different time steps for the DDA and IDA phases, because these processes have different maximum contact line velocities $\dot{R}_d$. Choosing different time steps requires interpolating $t_b(r)$ when evaluating the integral given by Eq. (77) (we used a linear method).

A.4. Comparison to an analytical solution for the DDA phase

Denesuk et al. (1993) derived an analytical solution for the case where the contact angle between the droplet and the surface of the porous medium, θ, remains constant. The drawing radius R_d decreases as follows (see Eq. (15) in Denesuk et al., 1993):

$$R_d = R_d(0)\left(1 - \sqrt{\frac{t}{\tau_{DDA}}}\right) \quad (79)$$

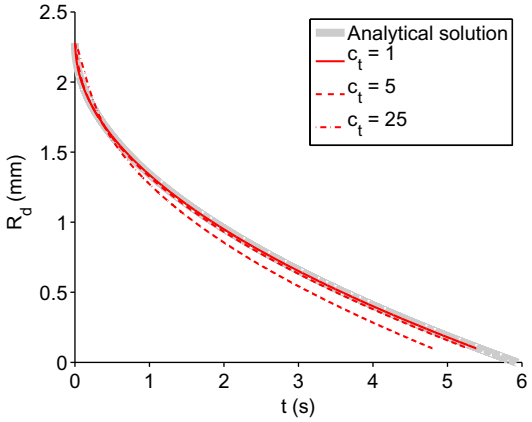

Fig. 14. Validation of our computer code by comparison to an analytical solution for the case where only the DDA phase is assumed. For $c_t \to 0$, our simulations converge to the analytical solution given by Eq. (79). Simulation parameters: $\theta_i = \theta_r = 25°$, $R_t = 0.1$ mm, $R_0 = 1$ mm, $\alpha = 0°$, $\epsilon = 0.3$, fluid properties of silicone oil.

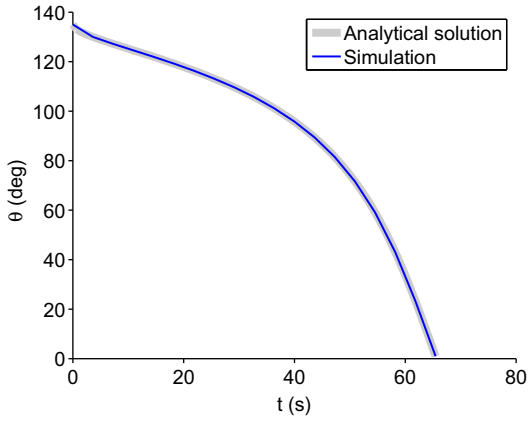

Fig. 15. Validation of our computer code by comparison to an analytical solution for the case where only the CDA phase is assumed. Our simulation reflects the analytical solution given by Eq. (81). Simulation parameters: $\theta_0 = \theta_a = 135°$, $\theta_r = 0°$, $R_t = 0.1$ mm, $R_0 = 1$ mm, $\alpha = 0°$, $\epsilon = 0.3$, fluid properties of silicone oil.

where

$$\tau_{DDA} = [\xi(\theta)]^{4/3}V_0^{2/3}\left(\frac{3}{\pi\epsilon A}\right)^2 \quad (80)$$

is the duration of infiltration. The analytical solution of Denesuk et al. (1993) allows validating our computer code for solving droplet infiltration during the DDA phase. Our model should approximate the Denesuk et al. (1993) solution, if we use Eq. (21) for dynamic contact angle and let $c_t \to 0$, because then $\theta(t) \to \theta_r$. Fig. 14 shows that this is indeed the case.

A.5. Comparison to an analytical solution for the CDA phase

Denesuk et al. (1993) obtained an analytical solution for the case where $\theta_r = 0$ and only the CDA phase occurs. We slightly generalize their solution to allow for $\theta_r \geqslant 0$. As $R_d(t) = \text{const.} = R_d(0)$ during the CDA phase, Eq. (37) becomes:

$$\theta(t) = \xi^{-1}\left(\frac{1}{R_d^3(0)}\left[V_0 - \pi A\epsilon R_d^2(0)\sqrt{t}\right]\right) \quad (81)$$

Infiltration is finished at time

$$\tau_{CDA} = t_r = \left(\frac{V_0 - R_d^3(0)\xi(\theta_r)}{\pi A\epsilon R_d^2(0)}\right)^2 \quad (82)$$

As it should, our t_r agrees with Eq. (14) in Denesuk et al. (1993) if $\theta_r = 0$. Fig. 15 shows that our computer code accurately reflects the analytical solution for the CDA phase.

References

Alleborn, N., Raszillier, H., 2004. Spreading and sorption of a droplet on a porous substrate. Chem. Eng. Sci. 59, 2071–2088.

Anderson, D.M., 2005. Imbibition of a liquid droplet on a deformable porous substrate. Phys. Fluids 17, 087104.

Bachmann, J., Woche, S.K., Goebel, M.-O., Kirkham, M.B., Horton, R., 2003. Extended methodology for determining wetting properties of porous media. Water Resour. Res. 39, 11-1–11-14.

Bacri, L., Brochard-Wyart, F., 2000. Droplet suction on porous media. Eur. Phys. J. E 3, 87–97.

Chebbi, R., 2007. Dynamics of liquid penetration into capillary tubes. J. Colloid Interf. Sci. 315, 255–260.

Clarke, A., Blake, T.D., Carruthers, K., Woodward, A., 2002. Spreading and imbibition of liquid droplets on porous surfaces. Langmuir 18, 2980–2984.

Cox, R.G., 1986. Dynamics of the spreading of liquids on a solid surface. Part 1: Viscous flow. J. Fluid Mech. 168, 169–194.

Daniel, R.C., Berg, J.C., 2006. Spreading on and penetration into thin, permeable print media: application to ink-jet printing. Adv. Colloid Interf. Sci. 123–126, 439–469.

Davis, S.H., Hocking, L.M., 2000. Spreading and imbibition of viscous liquid on a porous base. II. Phys. Fluids 12, 1646–1655.

de Gennes, P.G., Hua, X., Levinson, P., 1990. Dynamics of wetting: local contact angles. J. Fluid Mech. 212, 55–63.

Denesuk, M., Smith, G.L., Zelinski, B.J.J., Kreidl, N.J., Uhlmann, D.R., 1993. Capillary penetration of liquid droplets into porous materials. J. Colloid Interf. Sci. 158, 114–120.

Hoffman, R.L., 1975. A study of the advancing interface. J. Colloid Interf. Sci. 50, 228–241.

Holman, R.K., Cima, M.J., Uhland, S.A., Sachs, E., 2002. Spreading and infiltration of inkjet-printed polymer solution droplets on a porous substrate. J. Colloid Interf. Sci. 249, 432–440.

Jiang, T.S., Oh, S.-G., Slattery, J.C., 1979. Correlation for dynamic contact angle. J. Colloid Interf. Sci. 69, 74–77.

Leger, L., Joanny, J.F., 1992. Liquid spreading. Rep. Prog. Phys. 55, 431–486.

Linz, P., 1985. Analytical and numerical methods for Volterra equations. SIAM Stud. Appl. Math. 7.

Press, W.H., Flannery, B.P., Teukolsky, S.A., Vattering, W.T., 1992. Numerical Recipes: The Art of Scientific Computing. Cambridge University Press, London.

Šikalo, Š., Wilhelm, H.-D., Roisman, I.V., Jakirlić, S., Tropea, C., 2005. Dynamic contact angle of spreading droplets: experiments and simulations. Phys. Fluids 17, 2103+. doi: 10.1063/1.1928828.

Washburn, E.W., 1921. The dynamics of capillary flow. Phys. Rev. 17, 273–283.

Zadrazil, A., Stepanek, F., Matar, O.K., 2006. Droplet spreading imbibition and solidification on porous media. J. Fluid Mech. 562, 1–33.

Zhdanov, S.A., Starov, V.M., Sobolev, V.D., Velarde, M.G., 2003. Spreading of aqueous SDS solutions over nitrocellulose membranes. J. Colloid Interf. Sci. 264, 481–489.